

Review

III-Nitride Short Period Superlattices for Deep UV Light Emitters

Sergey A. Nikishin

Nano Tech Center, Department Electrical and Computer Engineering, Texas Tech University, Lubbock, TX 79423, USA; sergey.a.nikishin@ttu.edu; Tel.: +1-806-834-8807

Received: 17 October 2018; Accepted: 20 November 2018; Published: 23 November 2018



Featured Application: Advanced infrared, visible, and ultraviolet light emitters.

Abstract: III-Nitride short period superlattices (SPSLs), whose period does not exceed ~2 nm (~8 monolayers), have a few unique properties allowing engineering of light-emitting devices emitting in deep UV range of wavelengths with significant reduction of dislocation density in the active layer. Such SPSLs can be grown using both molecular beam epitaxy and metal organic chemical vapor deposition approaches. Of the two growth methods, the former is discussed in more detail in this review. The electrical and optical properties of such SPSLs, as well as the design and fabrication of deep UV light-emitting devices based on these materials, are described and discussed.

Keywords: III-nitrides; short period superlattices; light emitters

1. Introduction

The invention of semiconductor double heterostructure laser [1,2] and the concept of a semiconductor superlattice (SL) [3] can be considered as the foundation of modern semiconductor p–n junction-based light emitters, lasers, and light-emitting diodes. Double heterostructure (DHS) is a semiconductor “sandwich” where a layer of narrow band gap semiconductor (referred to as an active layer or a well, depending on its thickness) is placed between n-type and p-type layers (cladding layers) of the wide bandgap semiconductors. Under forward bias, the electrons and holes are injected from the cladding layers into an active layer, and well confined there. Confinement of these injected carriers leads to very effective radiative recombination in direct bandgap semiconductors.

The SL periodic layered structure of different crystalline semiconductors, allows for engineering of a bandgap of active (referred as a well) and cladding (referred as a barrier) layers when their thickness is of about a few nanometers. Note, these structures must be grown into two-dimensional (2D) growth mode, in order to get a flat/abrupt interface between all layers. The SLs based on the direct bandgap semiconductors in different combinations with p–n DHS are used for design and fabrication of light emitters operating in very wide range of wavelengths, ensuring the needs of optical communication, medicine, security, lighting, and agriculture [4–11]. We will discuss only p–n junction-based structures in this review.

III-Nitrides, AlN ($E_g = 6.2$ eV, [12,13]), GaN ($E_g = 3.4$ eV, [13]), InN ($E_g = 0.7$ eV, [14–16]), and their AlGaInN, AlGaIn, AlInN, InGaIn alloys, are direct bandgap semiconductors which would significantly influence the development of new optoelectronic and light-emitting devices throughout the 21st century [17–19]. Most III-nitride (III-N) light-emitting and laser diodes contain different SLs with a period exceeding 4 nm [20–23]. These SLs, in addition to the bandgap engineering, allow for reducing the dislocation density propagating into an active layer of III-N light-emitting diodes (LEDs) grown on the heavily lattice-mismatched substrates, like silicon and sapphire [24–26]. Strain engineering in an active layer of LEDs allows for modification of an internal quantum efficiency of radiative carrier

recombination [27,28]. The design and fabrication of such light emitters, based on “long period” SLs, are well described in many books and reviews [29–36].

III-N LEDs based on very short period superlattices (SPSLs, sometimes referenced as digital alloys, DA), periodic structures of GaN/AlN, AlGaInN/AlN, InGaInN/AlN, InGaInN/GaN, InN/GaN, and InAlN/GaN having a few monolayer thick wells and barriers, and a period not exceeding 2 nm, are very attractive for the design and fabrication of a new generation of light emitters. The main important difference between SPSLs and SL with a long period, is that carriers tunneling through barriers between quantum wells (QWs) in SPSLs already affect energy levels, and even lead to the formation of minibands (at least in the conduction band). Bandgap behavior of the InGaInN/GaN, InN/GaN, and InAlN/GaN SPSLs, and their applications in visible and infrared light emitters, are well summarized in recent publications [37–40]. The GaN/AlN, AlGaInN/AlN, and AlGa(In)N/AlN ($C_{In} < 0.02$ mol fraction) SPSLs are very attractive for deep ultraviolet light emitters [41–48]. One of the attractive features of AlGa(In)N/AlN SPSLs relates to the formation of very sharp heterointerfaces over the entire range of compositions, which makes it possible to obtain well/barrier thicknesses comparable to the interatomic distance, and to make tunneling the main carrier transport mechanism. For InGaInN/GaN structures, for example, the roughness of heterointerfaces increases if the composition of In approaches ~20%, which is important for practical applications, since carrier tunneling is difficult. This review aims to summarize the most significant efforts demonstrated in this field since 2002, when the first LED based on AlGa(In)N/AlN SPSLs operating at 280 nm, was demonstrated [41,42].

2. Growth and Structural Characterization

Most of III-N SPSLs for deep UV light emitters were grown using both molecular beam epitaxy (MBE) [41–43] and metal organic chemical vapor deposition (MOCVD) [37,44] methods on (0001) sapphire, Si (111), and (0001) GaN/sapphire template substrates. The detailed analysis of deep UV LED efficiency (internal and external), grown on different substrates, can be found in ref. [44].

One well-known advantage of MBE over MOCVD is the in situ monitoring of the growth process using the reflection high energy electron diffraction (RHEED) [49]. Analysis of the RHEED patterns in real time allows for controlling, at the monolayer (ML) scale, the structural properties of any substrate at the onset of epitaxy, the nucleation process and growth mode of the epitaxial layer, the growth rate of III-N compounds, and the composition of their alloys, by monitoring the period of RHEED intensity oscillations during deposition [50–52]. This statement can be illustrated by a few RHEED patterns.

The evolution of RHEED patterns illustrating the onset of gas source MBE (GSMBE) with ammonia on bulk (0001) AlN substrate is shown in Figure 1. As seen in Figure 1a, there are two types of reflections indicated separately by black solid and white dashed arrows. It was shown that this complex RHEED pattern can be attributable to the presence of Al₂O₃ surface islands [53]. The well-defined (00), (01), and (−01) reflections indicated by solid arrows can be attributed to the (1 × 1) AlN (0001) surface reconstruction at low temperatures. The weak additional reflections, indicated by dashed arrows, arise from formation of crystalline Al₂O₃ islands on the AlN surface. These islands cannot be removed by baking of the AlN substrate at high temperatures, up to ~1100 °C [53]. However, nitridation of such a surface, by exposing it to the flux of ammonia for a few minutes at a substrate temperature of ~800 °C, yields formation of a pure (1 × 1) surface structure on AlN (0001), as shown in Figure 1b. This (1 × 1) surface reconstruction was stable up to 900 °C. At this temperature, AlN, Al_{0.6}Ga_{0.4}N, and SPSL of AlN (3 ML)/Al_{0.08}Ga_{0.92}N (3 ML), with a total of 100 pairs, were successfully grown. The entire SPSL was grown in the 2D mode, and formation of a (2 × 2) surface reconstruction is shown in Figure 1c. The surface was very flat, with the root mean square (rms) roughness of less than 1 nm, as measured by 1 × 1 μm² scans, using atomic force microscopy.

Figure 2 shows the evolution of the RHEED patterns illustrating 2D→3D→2D growth mode transitions during ammonia GSMBE of Al_{0.55}Ga_{0.45}N (barrier)/Al_{0.45}Ga_{0.55}N (well) structure on Al_{0.55}Ga_{0.45}N/AlN buffer grown on (0001) sapphire substrate [54,55].

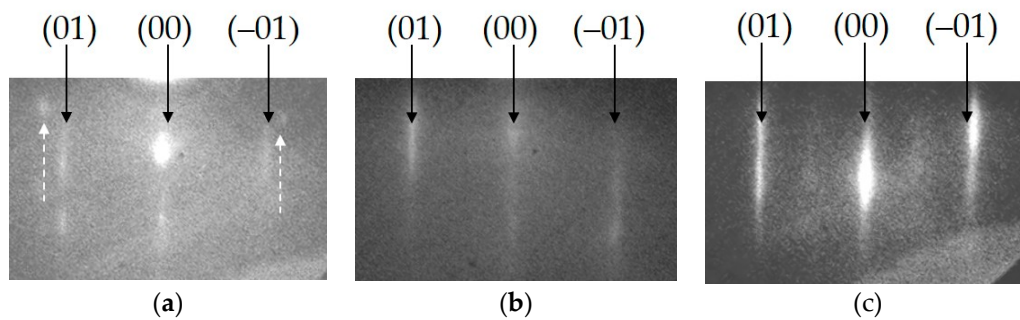


Figure 1. Evolution of reflection high energy electron diffraction (RHEED) patterns for different stages at onset of gas source molecular beam epitaxy (GSMBE). (a) The surface of (0001) AlN substrate at low temperatures. The (00), (01), and (−01) reflections from the (1 × 1) AlN surface and reflections from crystalline Al₂O₃ islands are indicated by arrows; (b) (1 × 1) surface reconstruction of AlN exposed to ammonia; (c) (2 × 2) surface structure after deposition of about 20 pairs of short period superlattices (SPSLs).

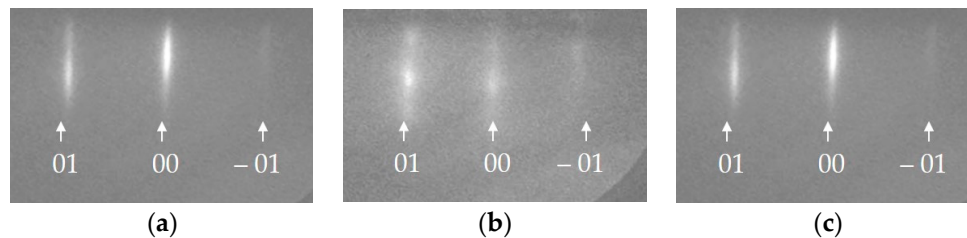


Figure 2. Evolution of RHEED patterns illustrating 2D and 3D growth modes at different (Al + Ga)/NH₃ flux ratios: (a) 2D-grown barrier at 20 sccm of ammonia; (b) 3D-grown well at 5.5 sccm of ammonia; (c) next 2D-grown barrier at 20 sccm of ammonia on a 3D-grown well.

All the barrier layers were grown in 2D growth mode with 1 × 1 surface reconstruction, as shown in Figure 2a, when an ammonia flux was sustained at 20 sccm. The wells grown under the same ammonia flux also demonstrated 2D growth mode. This mode was maintained at ammonia fluxes greater than 7 sccm (N-rich conditions), at a substrate temperature of 795 °C. With the ammonia flux reduced to 5.5 sccm, the RHEED patterns become quite spotty, as shown in Figure 2b. This behavior of the RHEED pattern is typical when the growth mode changes from 2D to 3D [56]. These growth conditions can be attributed to the “metal (Ga, Al)-rich” conditions, although additional experiments are required. It was shown that the barrier layer recovers when ammonia flux increased to 20 sccm and the RHEED pattern shows 2D growth mode, as shown in Figure 2c, by the time the next well is grown. Note that significant increase in the deep UV cathodoluminescence (CL) and photoluminescence (PL) emission from such grown structures was observed [57]. The increase was attributed to the formation of quantum dots (QDs) within the wells. It was concluded that the greatest CL intensity and longest PL lifetime for these structures are due to formation of quantum well (QW)/QD regions in Al_xGa_{1−x}N/Al_yGa_{1−y}N (0.3 < x < 0.45, 0.53 < y ≤ 1) QW structures [57,58]. The approach described in [54,55,57,58] was recently adjusted for a plasma-assisted MBE (PAMBE), and successfully used in an active layer of deep UV LEDs emitting at 232 nm [59]. The emission at 219 nm from PAMBE-grown 2 ML thick GaN QDs was also observed [60].

Analyzing the state-of-the-art results mentioned above and discussed in literature within last two to three years, we can conclude that one of the main current trends aimed at improving internal quantum efficiency (IQE) and external quantum efficiency (EQE) of UV LEDs is the creation of a low defective and highly efficient active layer in such structures. Future research should focus on finding the optimal ratio and distribution of QDs in the active layer, as well as on the development of the growth of LED structures on relatively inexpensive templates or bulk AlN substrates. Of course, it is much more effective to design and develop such an active layer using MBE, which provides in

situ monitoring of the growth process. Despite the fact that the MOCVD process dominates in the industrial growth of such structures, the results obtained using the MPE should make it possible to identify the most important structural and morphological factors influencing the radiative efficiency of the active layer of the LED. These new concepts can then be transferred to the MOCVD processes.

High resolution X-ray diffraction (HR-XRD) of AlN/AlGa_xN, AlN/GaN, and AlGa_xN/InGa_xN were carried out by many researchers [61–65] in order to estimate strain and dislocation density.

Note, HR-XRD measurements, in conjunction with Raman measurements, allow for estimation of the residual strain in SPSLs more precisely [66–69]. Usually, HR-XRD studies are carried out using a high-resolution diffractometer in double- and triple-axis alignment. A long range 2θ-ω scan of the (0002) reflection is shown in Figure 3 for a typical AlN/Al_xGa_{1-x}N SPSL grown on (0001) Al_{0.4}Ga_{0.6}N/AlN/sapphire template. Individual peaks corresponding to the AlN and Al_{0.4}Ga_{0.6}N buffer layers, and the 0th, ±1, and ±2 satellites of the SPSL are well defined in Figure 3. The average SPSL composition, 0.68, was determined from the 2θ position of the 0th peak [61]. From the position of the 0th and ±1 satellite peaks, the average period of the SPSL was determined to be 2.236 nm. Using the experimentally determined period, and assuming well composition of Al_{0.08}Ga_{0.92}N and pure AlN barriers, the well and the barrier thicknesses are found to be 0.808 nm and 1.428 nm, respectively [61]. Simulations based on the experimentally determined SPSL parameters yield an excellent fit to the experimental data, as shown in Figure 3. The deviation of the well and barrier thicknesses from their integer lattice parameters (integer ML multiples) can be attributed to many factors, including residual strain in the SPSL, formation of interfacial layers, interface roughness, composition fluctuations in the well and barrier, stacking faults (SFs), and inversion domain boundaries (IDBs). The detailed analysis of significance of all these factors was conducted in reference [61].

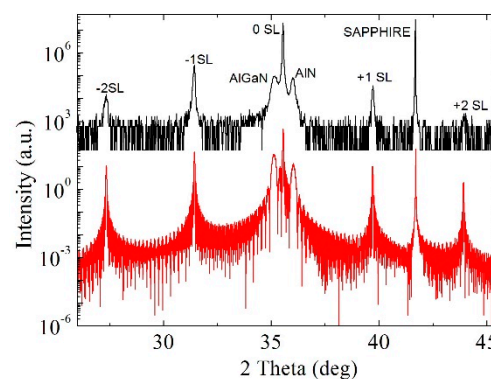


Figure 3. A long range 2θ-ω scan of (0002) reflection for AlN/Al_xGa_{1-x}N (0.07 < x < 0.09) obtained using a hybrid X-ray mirror. Black line—data [61], red line—simulations (courtesy of Dr. A. Chandolu).

Crystalline microstructure of any semiconductor is a very important factor influencing the performance of all light emitters. Cross-sectional structure of SPSLs should be investigated by transmission electron microscopy (TEM), in order to get a nanoscale resolution. Two TEM cross-sections of AlN/AlGa_xN SPSL, grown by GSMBE, are shown in Figure 4. Although the growth conditions (substrate temperature, flux ratio, growth time) were the same, the crystalline quality of these SPSLs were very different. It is clearly seen that SPSL grown directly on sapphire substrate contains a very high density of inversion domain boundaries (IDBs). These domains start to grow from substrate/layer interface, mostly due to incomplete nitridation of sapphire at the onset of epitaxial growth [45,70]. It was shown [71] that IDBs dominate the light emission process in GaN containing these defects. A similar result was reported for MBE grown AlGa_xN/GaN SLs [72]. However, SPSLs with high density of IDBs have inferior electrical properties [45] and cannot be used in the preparation of light-emitting devices. The most detailed impact of sapphire nitridation on the formation of inverse domains in AlN layers grown by MOCVD was discussed in a recent paper [70].

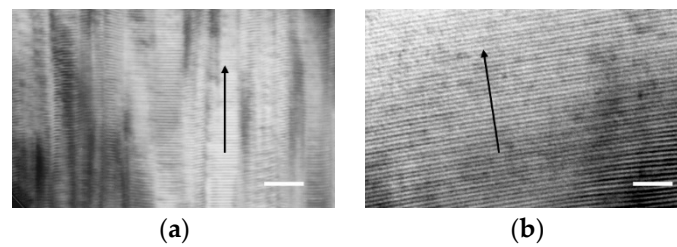


Figure 4. TEM cross-section of AlN/AlGaIn SPSLs (courtesy of Dr. S. N. G. Chu) (a) grown directly on bare (0001) sapphire; (b) grown on ~50 nm thick AlN buffer layer. The white scale bars are 20 nm long. The [0001] direction is shown by black arrows.

3. Bandgap of AlN/AlGa(In)N SPSLs

The bandgap structure of III-Ns SPSLs convenient for the deep UV light emitters can be simulated using different software [73–75]. The BESST (Bandgap Engineering Superlattice Simulation Tool) commercially available package from STR Inc. [76] was used to analyze the results of different teams [77,78], as well as most of our experimental results. This software is suitable for modelling optoelectronic devices utilizing SPSLs as essential units of their heterostructure designs. The BESST calculates the SPSL electron and hole minibands using a tight-binding approach and numerical solution of the Schrödinger equation with account of complex valence band structure of III-nitride compounds. Coupled solution of the Poisson equation for electric potential, accounting for polarization charges at the heterostructure interfaces, and discrete drift-diffusion transport equations, allows building up the band diagram of a device at an arbitrary bias and calculating the corresponding electron and hole currents, as well as the radiative recombination rate and emission spectrum. Field-dependent mobilities of electrons and holes used in the transport equations are found, self-consistently, with the simulated minibands of SPSLs.

Fourier-transform infrared optical reflectance (FTIR) [79–82], photoluminescence (PL) [83–85], and cathodoluminescence (CL) [41,42,86] are widely used to estimate the effective bandgaps of AlN/Ga(Al,In)N SPSLs. At room temperature, these methods are mostly qualitative, although still very useful for express control and adjustment of light-emitter properties during fabrication. The room temperature FTIR and CL were successfully used to facilitate fabrication of the first deep UV LEDs operating at 280 nm using undoped and n- and p-type AlN/Al_xGa_{1-x}N SPSLs [41,42].

As an example, the experimental FTIR and CL effective bandgaps of AlN/Al_{0.08}Ga_{0.92}N SPSLs and simulations of these structures obtained using two different approaches [46,76] are shown in Figure 5. One can see that both simulations provide the slope of the optical energy gap dependence on the SPSL period (actually, on the AlN barrier “effective” width), similar to that obtained by CL, whereas FTIR data demonstrate a different slope. This may have originated from the fact that FTIR measures the spectral dependence of light absorption, which may involve higher electron minibands and lower hole minibands or levels, whereas luminescence occurs mainly from the ground state minibands, due to their dominant occupation. Simulations by BESST show that SPSLs, regarded here, possess two different electron minibands and up to three heavy- and light-hole minibands, which can be considered as single energy levels at large SPSL periods because of miniband narrowing. Hence, contribution of the extra minibands to the light absorption may explain the difference in the optical energy gap determination by FTIR and CL.

Of course, the Stokes shift, which is related to the excited state configuration in the well material, is a factor in all radiative recombination processes and, therefore, should also yield to red shift of the CL’s estimated bandgap. Note that scatter in the experimental data shown in Figure 5 can be attributed to monolayer level uncertainty in the well and barrier thickness across the wafer, as well to local composition fluctuations in the well alloy [61,65].

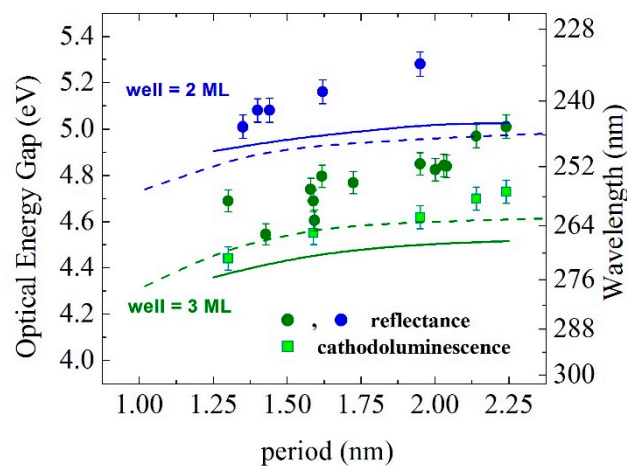


Figure 5. Experimental optical reflectance and cathodoluminescence (CL)-obtained effective bandgaps of AlN/Al_{0.08}Ga_{0.98}N SPSLs vs its period, grown with two nominal well thicknesses (2 and 3 monolayers (MLs), blue and green symbols, respectively) [45]. Theoretical simulations based on two approaches [46,76] are shown by continuous dashed and solid curves, respectively.

4. AlN/AlGa(In)N SPSL Doping and Ohmic Contacts

The efficiency of deep UV LEDs is very sensitive to the doping level of p- and n-type emitters. There are no significant issues with n-type doping of III-Ns compounds and their alloys, since Si, a common n-type dopant, behaves as a shallow donor, even in wide bandgap AlGa_xN alloys [87]. Although the activation energy of Si significantly increases in AlN [88–90], the resistivity of Si-doped AlN/Al_xGa_{1-x}(In)N (0.05 < x < 0.1) SPSLs is very low, 0.015–0.040 Ω·cm, and the electron concentration exceeds 10¹⁹ cm⁻³ [42,91]. Such n-type SPSLs can also be used as contact layers. Using a Ti/Al/Ti/Au stack annealed at 700 °C, specific contact resistance of the order of 10⁻⁵ Ω·cm² was obtained for AlN/AlGa(In)N SPSL with ~5.1 eV bandgap [92].

Unfortunately, for III-Ns compounds and their alloys, there is only one convenient p-type dopant, Mg, the experimentally determined activation energy of which varies from ~120 to ~220 meV in GaN [93,94], and reaches more than 500 meV in AlN [94,95]. A detailed analysis of the Mg activation energy in p-AlGa_xN epitaxial layers over the entire composition range was recently published [96]. It should be noted that if Mg-doped AlGa(In)N is grown using MOCVD, then Mg activation is required. This can be done by both rapid thermal annealing at elevated temperatures [97,98] and holding the sample under an electron beam irradiation [98–101]. It was also shown that Mg–O co-doping reduces acceptor activation energy in GaN [102,103], as in AlN [104]. However, this method of doping is not widely used since oxygen can react with aluminum and gallium, forming undesirable oxides of these metals, especially when used in molecular beam epitaxy.

The hole density at room temperature in Al_xGa_{1-x}N:Mg alloys with Mg concentration at ~10¹⁹–10²⁰ cm⁻³ is shown in Figure 6a. Note that all Mg concentrations were obtained using secondary ion mass spectrometry (SIMS) [25,103].

A significant decrease in the hole concentration with an increase in the Al content in AlGa_xN is consistent with an increase in the activation energy of Mg in the wide bandgap layers. For AlN/Al_xGa_{1-x}(In)N (0.03 < x < 0.08) SPSLs with 2–3 ML thick wells, and periods of the order of 6–8 MLs, the average AlN concentration in SPSLs can be changed in the range of $y_{ave} = 0.5$ –0.8. The average Mg concentration in these SPSLs is usually at the level of 10¹⁹ cm⁻³. The concentration of holes can be at the level of 10¹⁸ cm⁻³, even in SPSLs with high average AlN content, as is seen in Figure 6a. Such structures were obtained using both MBE and MOCVD methods [25,41,42,45,91,105–110].

Figure 6b shows the results of temperature-dependent Hall characterization of three SPSLs and one AlGa_xN layer. The Mg concentration was ~10¹⁹ cm⁻³ in SPSLs, and ~3 × 10¹⁹ cm⁻³ in AlGa_xN.

Note that the composition of the well was in the range $0.03 < x < 0.08$ which is very similar to the Al concentration in the AlGaInN thick layer. Average AlN concentrations of these SPSLs were $y_{ave} = 0.65, 0.55,$ and 0.45 . The average SPSL compositions, y_{ave} , were obtained using X-ray diffraction [61]. The hole density, here, corresponds to the hole concentration averaged over the full SPSL thickness. Fitting lines 1, 2, and 3 were calculated using BESST simulator, assuming AlN barriers in the SPSL to be relaxed. It is clearly seen that the hole concentration varies very little with the temperature in SPSLs, and is highly dependent on the temperature (almost 1.5 orders of magnitude) in a uniformly Mg-doped $Al_{0.05}Ga_{0.95}N$ layer. Similar experimental results were reported by many different teams [45,105–115].

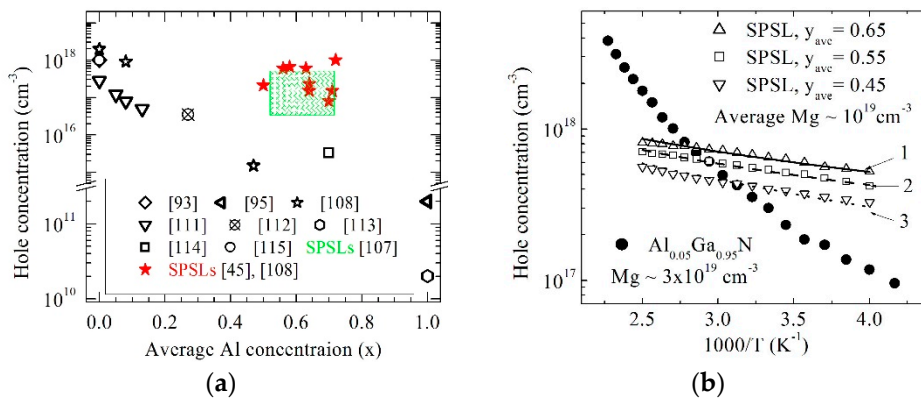


Figure 6. Hole concentration in $Al_xGa_{1-x}N$ alloys and AlN/AlGa(In)N SPSLs. (a) The dependence on average Al concentration in epitaxial layers (black symbols) and in SPSLs (red symbols and green box); (b) The temperature dependence of the hole concentration in $Al_{0.05}Ga_{0.95}N$ epitaxial layer (~0.5 μm thick, filled circles) and in AlN/ $Al_xGa_{1-x}N$ SPSLs (open symbols). Lines 1, 2, and 3 are the results of the applied BESST simulator [76].

The valence band edge profile in AlN (~0.90 nm)/ $Al_{0.03}Ga_{0.97}N$ (~0.52 nm) SPSL, computed by the BESST simulator [76] at room temperature, are shown in Figure 7. The position of the Fermi level in this SPSL corresponds to the zero-energy horizontal line shown in Figure 7a. The acceptor levels in $Al_{0.03}Ga_{0.97}N$ -well and AlN-barrier layers are indicated by the dashed lines.

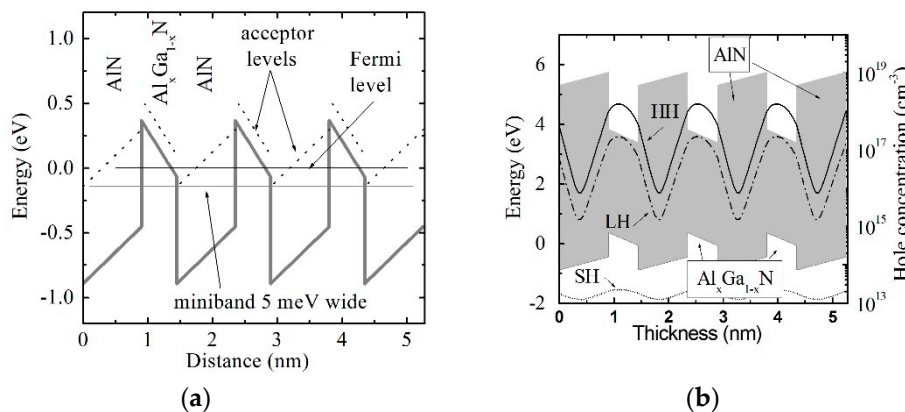


Figure 7. Valence band layout in AlN/ $Al_{0.03}Ga_{0.97}N$ SPSL, computed for room temperature (a) and band diagram and heavy (HH), light (LH), and split-off (SH) hole concentrations in this sample (b). The acceptor level positions were estimated by neglecting the effect of the hole confinement in the quantum wells.

It is clearly seen that the acceptor levels in the quantum wells are above the Fermi level. Thus, these acceptors should be not activated. In the AlN barriers, the Fermi level crosses the acceptor energy levels, yielding a partial activation of acceptors in these layers. The degree of activation depends

on temperature, creating hole tunneling from barriers to wells, which results in the exponential dependences of hole concentration, as shown in Figure 6.

Figure 7b shows the distributions of the heavy, light, and split-off holes in the same SPSL obtained by self-consistent solution of the Poisson and Schrödinger equations [76], accounting for the complex valence band structure of III-nitrides [116]. It is clearly seen that the total hole density in such an SPSL mostly depends on the heavy hole concentration. The contribution of the split-off holes can be neglected, due to the fact that this subband in the SPSL is far below the heavy and light subbands. Note, the holes in the SPSL are accumulated in the wells, partially penetrating into the AlN barriers.

One could conclude that the efficiency of Mg activation is a very weak function of temperature in wide bandgap AlN/Al_xGa_{1-x}(In)N SPSL (E_g from ~4.2 to ~5.3 eV) [107,108]. Thus, these SPSLs are very attractive for fabrication of transparent low resistive ohmic contacts for deep UV light emitters.

Various contact metallization schemes have been applied for Mg-doped p-GaN, including Au, Ni, Ti, Pd, Pt, Au/Ni, Au/Pt, Au/Cr, Au/Pd, Au/Mg/Au, Au/Pt/Pd, Au/Cr/Ni, Au/Pt/Ni, Au/Ni/Pt, Au-Zn/Ni, Si/Ni/Mg/Ni, etc. [117]. Oxidized Au/Ni is the most common ohmic contact to p-GaN, due to the relatively low specific contact resistance (ρ_c) and simplicity of fabrication [118]. It was shown that formation of crystalline NiO and Ni₃Ga₄ play an essential role in the reduction of the specific contact resistance of p-GaN [118–121]. While the formation of NiO yields a reduction of the specific contact resistance, the formation of Ni₃Ga₄ results in the eventual increase in the contact resistance [119–121]. The lowest specific contact resistance $\rho_c \sim 9.2 \times 10^{-6}$ and $2 \times 10^{-6} \Omega \text{ cm}^2$ at 150 °C were achieved for p-type Mg-doped GaN and Al_xGa_{1-x}N layers [121,122].

Similar approach was successfully used for fabrication of ohmic contacts on p-type AlN/Al_xGa_{1-x}N SPSLs [108]. Figure 8 shows the temperature dependence of the specific contact resistances, ρ_c , for three SPSLs with average AlN content of $y_{ave} \sim 0.7$ and for the ~300 nm thick Mg-doped p-Al_{0.03}Ga_{0.97}N epitaxial layer. The Mg concentration in all samples was $\sim 10^{19} \text{ cm}^{-3}$ and room temperature ρ_c was $\sim 4 \times 10^{-5} \Omega \cdot \text{cm}^2$.

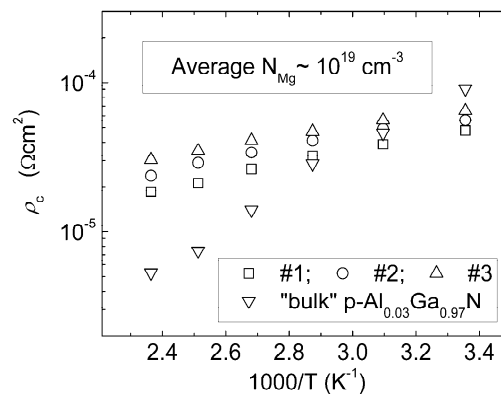


Figure 8. Specific contact resistances of Mg-doped AlN/Al_xGa_{1-x}N SPSLs ($y_{ave} \sim 0.7$) and Al_{0.03}Ga_{0.97}N epitaxial layer at different temperatures.

It was shown that the temperature dependence of the specific contact resistance is primarily controlled by the activation energy of Mg acceptors in Al_xGa_{1-x}N [123]. The ρ_c of metal/SPSL ohmic contact, as seen in Figure 8, also follows the temperature dependence of hole concentration in these structures, which are very similar to that shown in Figure 6b, since the density of acceptors activated in AlN barriers is the primary factor influencing the hole concentration in the well, producing a weaker temperature dependence compared to bulk materials. Thus, a weak dependence of ρ_c on temperature is expected, even when thermionic mechanism of current injection dominates in the metal/SPSL ohmic contact. This expectation agrees with the results shown in Figure 8.

5. Deep UV Light Emitters Based on AlN/AlGa(In)N SPSLs

The ability to change the bandgap in SPSL by several hundred meV, by changing the thickness of the well by 1 ML, opened up a very simple path to the implementation of the DHS LEDs. Since SPSL with particular barrier/well thicknesses has its effective bandgap, we can consider them to form a heterostructure in the sense that an SPSL-based active layer with a smaller effective bandgap is sandwiched between n- and p-type SPSL-based cladding layers with a larger bandgap.

A schematic cross-section of a typical DHS for a sub-300 nm LED is shown in Figure 9. The structure consists of six main parts: (1) thin, <100 nm, AlN buffer; (2) thick, ~200 nm, $\text{Al}_{0.7-0.8}\text{Ga}_{0.3-0.2}\text{N}$ buffer for reduction of dislocation density in a device structure (this layer can be replaced by AlN/GaN SPSL—“dislocation absorber”); (3) n-type AlN(5 ML)/ $\text{Al}_{0.92-0.97}\text{Ga}_{0.08-0.03}(\text{In})\text{N}$ (2 ML) SPSL cladding layer of ~400 nm; (4) undoped AlN(5 ML)/ $\text{Al}_{0.92-0.97}\text{Ga}_{0.08-0.03}(\text{In})\text{N}$ (3 ML) SPSL active region (5 pairs); (5) p-type AlN(5 ML)/ $\text{Al}_{0.92-0.97}\text{Ga}_{0.08-0.03}(\text{In})\text{N}$ (2 ML) SPSL cladding layer of ~200 nm; (6) thin, ~2–5 nm, p-type contact layer with the composition of SPSL’s well material or pure GaN:Mg. As can be seen from the TEM cross-section of this device, shown in the same Figure 9, the barrier/well interfaces are quite sharp, and the thickness of the well in the active region is greater than in the adjacent n- and p-type barriers.

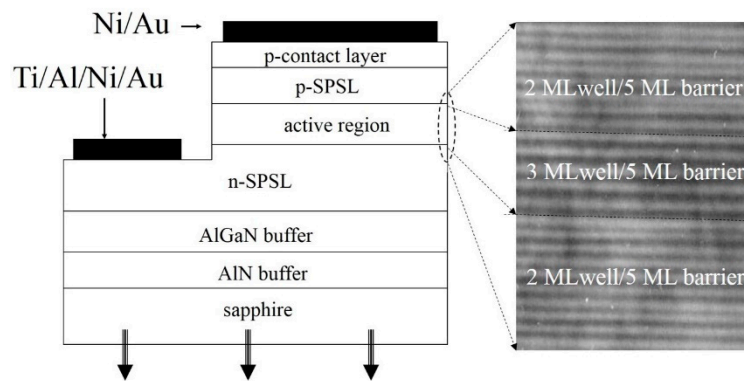


Figure 9. A not-in-scale schematic cross-section (on the left) of a double heterostructure (DHS) light-emitting diode (LED) and TEM cross-section (on the right) of the active region, and adjacent n- and p-type emitters of this diode.

The current–voltage (I–V) characteristic of a typical 260 nm DHS mesa-LED is shown in Figure 10a. The LED turns on at ~6.0 V, and has a relatively high differential series resistance R_{ser} of $115 \pm 5 \Omega$ under forward bias from 8 V to 12 V. The R_{ser} of mesa diodes is the sum of the contact (R_{cont}), spreading (R_{sp}), and vertical (R_{ver}) resistances. The contact resistance of a 160 μm diameter diode, obtained from specific contact resistance, is $R_{cont} \sim 90 \Omega$. The estimated spreading resistance of this LED is $R_{sp} \sim 20 \Omega$, taking into account the resistivity of n-type AlGaIn buffer layer (not shown in the inset of Figure 10a). The resistance of the etched part of the mesa, corresponding to transport across the SPSL layers, is $R_{ver} \approx \rho_1 \times (h/A)$ where ρ_1 is the perpendicular (along the growth direction) resistivity of the SPSL, h is the height of the mesa (~300 nm, with the thickness of p-SL ~200 nm), and A is the contact area. Finally, we obtain $R_{ver} \sim 5 \Omega$, resulting in $\rho_1 \sim 50 \Omega \text{ cm}$ for a p-type SPSL. Comparing this to the in-plane conductivity (ρ_2) of the p-type SPSL obtained from Hall measurements, $\rho_2 \sim 4 \Omega \text{ cm}$, we obtain the conductivity anisotropy $\rho_1/\rho_2 \sim 13$. These simple considerations indicate relatively low ρ_1 , considering the high AlN fraction in these SPSLs, and underscore the importance of reducing the contact resistance to p-type materials. However, it is also important to lower R_{sp} by optimization of the buffer layer thickness and its resistivity. Similar I–V characteristics were reported by different teams for LEDs emitting near the same deep UV range of the wavelengths [42–46,91–128].

The typical electroluminescence spectra of DHS LEDs based on AlN/AlGa(In)N SPSLs are shown in Figure 10b. All these spectra were obtained on LEDs with a similar geometry, and with the same currents. A significant decrease in EQE is evident for devices emitting in ever deeper UV. The external

quantum efficiency (EQE) of such simple LEDs does not exceed 0.1%. The absence of the electron blocking layer is the main drawback [129] of the structure shown in Figure 9. In order to increase the efficiency of such LED structures, it was proposed to insert a few monolayers-thick AlN electron blocking layer between the active layer and the p-emitter [35,36].

Summarizing, it should be noted that several new approaches to the use of SPSLs in combination with QDs in the active layer of the LED have been proposed [60,130–132]. The most promising, from my point of view, is the idea set forth in the ref. [60], where, experimentally, deep UV emission at 219 nm from ultrathin MBE-grown GaN/AlN quantum structure was demonstrated. I believe in the success of this approach, since we observed a similar effect almost 10 years ago [54,55,57,58].

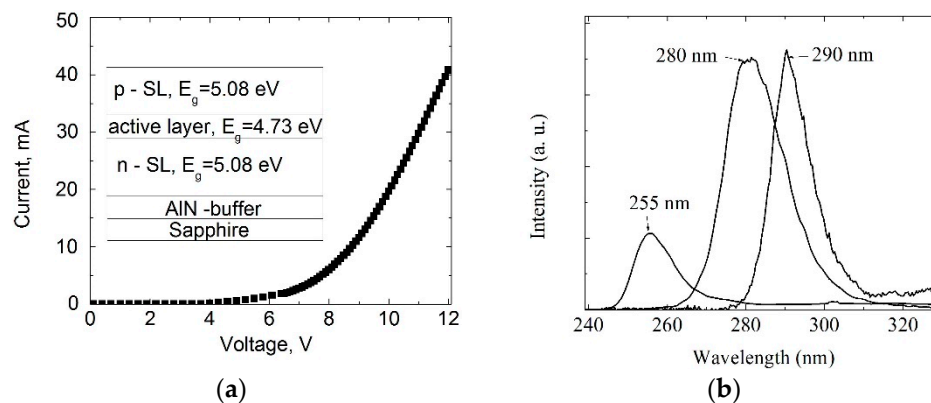


Figure 10. Electrical and optical characteristics of AlN/AlGa(In)N SPSL-based DHS mesa-LEDs. (a) Current–voltage characteristic of a typical LED operating at 262 nm wavelength. Note that light emission was observed with forward *dc* current above 2 mA; (b) Electroluminescence spectra of similar AlN/AlGa(In)N SPSL-based DHS mesa-LEDs operating at 255, 280, and 290 nm.

6. Conclusions

It was demonstrated that AlN/Al_xGa_{1-x}N p- and n-type SPSLs with average AlN content up to $y_{ave} \sim 0.7$ and bandgap over 5.1 eV could have hole and electron concentrations exceeding 10^{18} cm⁻³. Low-resistance ohmic contacts with specific contact resistance below $\sim 4 \times 10^{-5}$ Ω·cm² can be formed on these SPSLs. The LEDs based on SPSLs with emission wavelengths from 290 to 232 nm were demonstrated by different teams.

Funding: This paper received no external funding.

Acknowledgments: I would like to acknowledge all my colleagues involved in this research. I thank S. Yu. Karpov for very helpful discussions.

Conflicts of Interest: The author declares no conflict of interest.

References

1. Alferov, Z.I. Nobel Lecture: The double heterostructure concept and its applications in physics, electronics, and technology. *Rev. Mod. Phys.* **2001**, *73*, 767–782. [[CrossRef](#)]
2. Kroemer, H. Nobel Lecture: Quasielectric fields and band offsets: Teaching electrons new tricks. *Rev. Mod. Phys.* **2001**, *73*, 783–793. [[CrossRef](#)]
3. Esaki, L.; Tsu, R. Superlattice and negative differential conductivity in semiconductors. *IBM J. Res. Dev.* **1970**, *14*, 61–65. [[CrossRef](#)]
4. Casey, H.C., Jr.; Panish, M.B. *Heterostructure Lasers*; Academic Press: New York, NY, USA, 1978; pp. 156–300. ISBN 0-12-163102-8.
5. Ivanov, S.V.; Kopev, P.S.; Ledentson, N.N.; Meltser, B.Y.; Nadtochy, M.Y.; Ustinov, V.M.; Vasilev, A.M. Ultrathin layers and short-period superlattices in semiconductor structures. *Phys. Stat. Sol.* **1990**, *118*, 169–177. [[CrossRef](#)]

6. Chang, M.-H.; Das, D.; Varde, P.V.; Pecht, M. Light emitting diodes reliability review. *Microelectron. Reliab.* **2012**, *52*, 762–782. [[CrossRef](#)]
7. Opel, D.R.; Hagstrom, E.; Pace, A.K.; Sisto, K.; Hirano-Ali, S.A.; Desai, S.; Swan, J. Light emitting diodes, a brief review and clinical experience. *J. Clin. Aesthet. Dermatol.* **2015**, *8*, 36–44, PMID:PMC4479368. [[PubMed](#)]
8. Yadav, A.; Titkov, I.E.; Sokolovskii, G.S.; Karpov, S.Y.; Dudelev, V.V.; Soboleva, K.K.; Strassburg, M.; Pietzonka, I.; Lugauer, H.-J.; Rafailov, E.U. AlGaInP red-emitting light emitting diode under extremely high pulsed pumping. *Proc. SPIE* **2016**, 9768. [[CrossRef](#)]
9. Karpov, S.Y. Light-emitting diodes for solid-state lighting: Searching room for improvements. *Proc. SPIE* **2016**, 9768. [[CrossRef](#)]
10. Gupta, S.D. (Ed.) *Light Emitting Diodes for Agriculture*; Springer: Singapore, 2017. [[CrossRef](#)]
11. Schubert, E.F. *Light-Emitting Diodes*, 3rd ed.; Rensselaer Polytechnic Institute Troy: New York, NY, USA, 2018; pp. 17-1–17-15, 19-6–19-16, 21-2–21-8. ISBN 978-0-9863826-6-6.
12. Pantha, B.N.; Dahal, R.; Nakarmi, M.L.; Nepal, N.; Li, J.; Lin, J.Y.; Jiang, H.X.; Paduano, Q.S.; Weyburne, D. Correlation between optoelectronic and structural properties and epilayer thickness of AlN. *Appl. Phys. Lett.* **2007**, *90*. [[CrossRef](#)]
13. Zhou, C.; Ghods, A.; Saravade, V.G.; Patel, P.V.; Yungans, K.L.; Ferguson, C.; Feng, Y.; Kucukgok, B.; Lu, N.; Ferguson, I.T. Review—The current and emerging applications of the III-Nitrides. *ECS J. Sol. Stat. Sci. Technol.* **2017**, *6*, Q-149–Q-156. [[CrossRef](#)]
14. Davydov, V.Y.; Klochikhin, A.A.; Emtsev, V.V.; Kurdyukov, D.A.; Ivanov, S.V.; Vekshin, V.V.; Bechstedt, F.; Furthmüller, J.; Aderhold, J.; Graul, J.; et al. Band gap of hexagonal InN and InGaN alloys. *Phys. Stat. Sol.* **2002**, *234*, 787–795. [[CrossRef](#)]
15. Wu, J.; Walukiewicz, W.; Shan, W.; Yu, K.M.; Ager, J.W., III; Li, S.X.; Haller, E.E.; Lu, H.; Schaff, W.J. Temperature dependence of the fundamental band gap of InN. *J. Appl. Phys. Lett.* **2003**, *94*, 4457–4460. [[CrossRef](#)]
16. Andreev, B.A.; Kudryavtsev, K.E.; Yablonskiy, A.N.; Lobanov, D.N.; Bu shuykin, P.A.; Krasilnikova, L.V.; Skorokhodov, E.V.; Yunin, P.A.; Novikov, A.V.; Davydov, V.Y.; Krasilnik, Z.F. Towards the indium nitride laser: Obtaining infrared stimulated emission from planar monocrystalline InN structures. *Sci. Rep.* **2018**, *8*. [[CrossRef](#)] [[PubMed](#)]
17. Akasaki, I. Nobel Lecture: Fascinated journeys into blue light. *Rev. Mod. Phys.* **2015**, *87*, 1119–1131. [[CrossRef](#)]
18. Amano, H. Nobel Lecture: Growth of GaN on sapphire via low-temperature deposited buffer layer and realization of p-type GaN by Mg doping followed by low-energy electron beam irradiation. *Rev. Mod. Phys.* **2015**, *87*, 1133–1138. [[CrossRef](#)]
19. Nakamura, S. Nobel Lecture: Background story of the invention of efficient blue InGaN light emitting diodes. *Rev. Mod. Phys.* **2015**, *87*, 1139–1151. [[CrossRef](#)]
20. Kipshidze, G.; Kuryatkov, V.; Borisov, B.; Holtz, M.; Nikishin, S.; Temkin, H. AlGaInN light-emitting diodes grown on Si (111). *Appl. Phys. Lett.* **2002**, *80*, 3682–3684. [[CrossRef](#)]
21. Sizov, V.S.; Tsatsulnikov, A.F.; Sakharov, A.V.; Lundin, W.V.; Zavarin, E.E.; Cherkashin, N.A.; Hÿtch, M.J.; Nikolaev, A.E.; Mintairov, A.M.; He, Y.; et al. The use of short-period InGaN/GaN superlattices in blue-region light-emitting diodes. *Semiconductors* **2010**, *44*, 924–930. [[CrossRef](#)]
22. Lähnemann, J.; Ajay, A.; Den Hertog, M.I.; Monroy, E. Near-infrared intersubband photodetection in GaN/AlN nanowires. *Nano Lett.* **2017**, *17*, 6954–6960. [[CrossRef](#)] [[PubMed](#)]
23. Mehta, K.; Liu, Y.-S.; Wang, J.; Jeong, H.; Detchprohm, T.; Park, Y.J.; Alugubelli, S.R.; Wang, S.; Ponce, F.A.; Shen, S.-C.; et al. Lateral current spreading in III-N ultraviolet vertical-cavity surface-emitting lasers using modulation-doped short period superlattices. *IEEE J. Quant. Electron.* **2018**, *54*. [[CrossRef](#)]
24. Nikishin, S.A.; Faleev, N.N.; Antipov, V.G.; Francoeur, S.; Grave de Peralta, L.; Seryogin, G.A.; Temkin, H.; Prokofyeva, T.I.; Holtz, H.; Chu, S.N.G. High quality GaN grown on Si(111) by gas source molecular beam epitaxy with ammonia. *Appl. Phys. Lett.* **1999**, *75*, 2073–2075. [[CrossRef](#)]
25. Nikishin, S.; Kipshidze, G.; Kuryatkov, V.; Zubrilov, A.; Choi, K.; Gherasoiu, Iu.; Grave de Peralta, L.; Prokofyeva, T.; Holtz, M.; Asomoza, R.; et al. Gas source molecular beam epitaxy of high quality AlGaIn on Si and sapphire. *Mat. Res. Soc. Symp.* **2001**, 639. [[CrossRef](#)]

26. Xiao, M.; Zhang, J.; Hao, Y. High-quality Ga-rich AlGa_N grown on trapezoidal patterned GaN template using super-short period AlN/GaN superlattices for rapid coalescence. *J. Cryst. Growth* **2017**, *464*, 153–158. [[CrossRef](#)]
27. Aumer, M.E.; LeBoeuf, S.F.; Bedair, S.M.; Smith, M.; Lin, J.Y.; Jiang, H.X. Effects of tensile and compressive strain on the luminescence properties of AlInGa_N/InGa_N quantum well structures. *Appl. Phys. Lett.* **2000**, *77*, 821–823. [[CrossRef](#)]
28. Son, J.H.; Lee, J.-L. Strain engineering for the solution of efficiency droop in InGa_N/Ga_N light-emitting diodes. *Opt. Express* **2010**, *18*, 5466–5471. [[CrossRef](#)] [[PubMed](#)]
29. Nakamura, S.; Fasol, G. *The Blue Laser Diode*; Springer: Berglin/Heidelberg, Germany; New York, NY, USA, 1997; pp. 147–300. ISBN 978-3-662-03464-4 or 978-3-662-03462-0.
30. Morkoç, H. *Handbook of Nitride Semiconductors and Devices. V.3: GaN-Based Optical and Electronic Devices*; WILEY-VCH Verlag GmbH & Co. KGaA: Weinheim, Germany, 2009; pp. 4–334. ISBN 978-3-527-40839-9.
31. Kneissl, M.; Rass, J. *III-Nitride Ultraviolet Emitters Technology and Applications*; Springer Series in Materials Science; Springer: Berglin/Heidelberg, Germany, 2016; Volume 227, pp. 3–12, 90–104, ISBN 978-3-319-24098-5.
32. Amano, H. Progress and prospect of growth of wide-band-gap group III Nitrides. In *III-Nitride Based Light Emitting Diodes and Applications*, 2nd ed.; Seong, T.-Y., Han, J., Amano, H., Morkoç, H., Eds.; Springer: Singapore, 2017; pp. 1–9. ISBN 978-981-10-3754-2.
33. Egawa, T.; Oda, O. LEDs based on hetero epitaxial GaN on Si substrates. In *III-Nitride Based Light Emitting Diodes and Applications*, 2nd ed.; Seong, T.-Y., Han, J., Amano, H., Morkoç, H., Eds.; Springer: Singapore, 2017; pp. 1–9. ISBN 978-981-10-3754-2.
34. Tadatomo, K.; Okagawa, H.; Ohuchi, Y.; Tsunekawa, T.; Kudo, H.; Sudo, Y.; Kato, M.; Taguchi, T. High output power near-ultraviolet and violet light-emitting diodes fabricated on patterned sapphire substrates using metalorganic vapor phase epitaxy. *J. Light Vis. Env.* **2003**, *27*, 140–145. [[CrossRef](#)]
35. Kneissl, M.; Rass, J.; Schade, L.; Schwarz, U.T. Growth and Optical Properties of GaN-Based Non- and Semipolar LEDs. In *III-Nitride Based Light Emitting Diodes and Applications*, 2nd ed.; Seong, T.-Y., Han, J., Amano, H., Morkoç, H., Eds.; Springer: Singapore, 2017; pp. 93–128. ISBN 978-981-10-3754-2.
36. Hirayama, H.; Kamata, N.; Tsubaki, K. AlGa_N-Based Deep-Ultraviolet Light-Emitting Diodes. In *III-Nitride Based Light Emitting Diodes and Applications*, 2nd ed.; Seong, T.-Y., Han, J., Amano, H., Morkoç, H., Eds.; Springer: Singapore, 2017; pp. 93–128. ISBN 978-981-10-3754-2.
37. Staszczak, G.; Gorczyca, I.; Grzank, E.; Smalc-Koziorowska, J.; Targowski, G.; Czernecki, R.; Siekacz, M.; Grzanka, S.; Skierbiszewski, C.; Schulz, T.; et al. Bandgap behavior of InGa_N/Ga_N short period superlattices grown by metal-organic vapor phase epitaxy. *Phys. Stat. Sol.* **2017**, *254*, 1600710. [[CrossRef](#)]
38. Dimitrakopoulos, G.P.; Vasileiadis, I.G.; Bazioti, C.; Smalc-Koziorowska, J.; Kret, S.; Dimakis, E.; Florini, N.; Kehagias, T.; Suski, T.; Karakostas, T.; et al. Compositional and strain analysis of In(Ga)_N/Ga_N short period superlattices. *J. Appl. Phys.* **2018**, *123*, 024304. [[CrossRef](#)]
39. Gorczyca, I.; Suski, T.; Christensen, N.E.; Svane, A. Theoretical study of nitride short period superlattices. *J. Phys. Condens. Matter* **2018**, *30*, 063001. [[CrossRef](#)] [[PubMed](#)]
40. Lundin, W.V.; Nikolaev, A.E.; Sakharov, A.V.; Zavarin, E.E.; Valkovskiy, G.A.; Yagovkina, M.A.; Usov, S.O.; Kryzhanovskaya, N.V.; Sizov, V.S.; Brunkov, P.N.; et al. Single quantum well deep-green LEDs with buried InGa_N/Ga_N short-period superlattice. *J. Cryst. Growth* **2011**, *315*, 267–271. [[CrossRef](#)]
41. Kipshidze, G.; Kuryatkov, V.; Borisov, B.; Nikishin, S.; Holtz, M.; Chu, S.N.G.; Temkin, H. Deep Ultraviolet AlGaInN-Based Light-Emitting Diodes on Si(111) and Sapphire. *Phys. Stat. Sol.* **2002**, *192*, 286–291. [[CrossRef](#)]
42. Kipshidze, G.; Kuryatkov, V.; Zhu, K.; Borisov, B.; Holtz, M.; Nikishin, S.; Temkin, H. AlN/AlGaInN superlattice light emitting diodes at 280 nm. *J. Appl. Phys.* **2003**, *93*, 1363–1366. [[CrossRef](#)]
43. Jmerik, V.N.; Lutsenko, E.V.; Ivanov, S.V. Plasma-assisted molecular beam epitaxy of AlGa_N heterostructures for deep-ultraviolet optically pumped lasers. *Phys. Stat. Sol.* **2013**, *210*, 439–450. [[CrossRef](#)]
44. Shatalov, M.; Sun, W.; Jain, R.; Lunev, A.; Hu, X.; Dobrinsky, A.; Bilenko, Yu.; Yang, J.; Garrett, G.A.; Rodak, L.E.; et al. High power AlGa_N ultraviolet light emitters. *Semicond. Sci. Technol.* **2014**, *29*, 084007. [[CrossRef](#)]
45. Nikishin, S.A.; Holtz, M.; Temkin, H. Digital alloys AlN/AlGa_N for deep UV light emitting diodes. *Jpn. J. Appl. Phys.* **2005**, *44*, 7221–7226. [[CrossRef](#)]

46. Sun, W.; Tan, C.-K.; Tansu, N. AlN/GaN Digital alloy for mid- and deep-ultraviolet optoelectronics. *Sci. Rep.* **2017**, *7*, 11826–11833. [[CrossRef](#)] [[PubMed](#)]
47. Gorczyca, I.; Suski, T.; Strak, P.; Staszczak, G.; Christensen, N.E. Band gap engineering of In(Ga)N/GaN short period superlattices. *Sci. Rep.* **2017**, *7*, 16055. [[CrossRef](#)] [[PubMed](#)]
48. Kaneko, M.; Ueta, S.; Horita, M.; Kimoto, T.; Suda, J. Deep-ultraviolet light emission from 4H-AlN/4H-GaN short-period superlattice grown on 4H-SiC (11–20). *Appl. Phys. Lett.* **2018**, *112*, 012106. [[CrossRef](#)]
49. Neave, J.H.; Joyce, B.A.; Dobson, P.J.; Norton, N. Dynamics of films growth of GaAs by MBE from RHEED observations. *Appl. Phys. A* **1983**, *31*, 1–8. [[CrossRef](#)]
50. Yang, Z.; Li, L.K.; Wang, W.I. High-quality GaN and AlN grown by gas-source molecular beam epitaxy using ammonia as the nitrogen source. *J. Vac. Sci. Technol. B* **1996**, *14*, 2354–2356. [[CrossRef](#)]
51. Grandjean, N.; Massies, J. GaN and Al_xGa_{1-x}N molecular beam epitaxy monitored by reflection high-energy electron diffraction. *Appl. Phys. Lett.* **1997**, *71*, 1816–1818. [[CrossRef](#)]
52. Daudin, B.; Widmann, F. Layer-by-layer grown of AlN and GaN by molecular beam epitaxy. *J. Cryst. Growth* **1997**, *182*, 1–5. [[CrossRef](#)]
53. Nikishin, S.A.; Borisov, B.A.; Chandolu, A.; Kuryatkov, V.V.; Temkin, H.; Holtz, M.; Mokhov, E.N.; Makarov, Y.; Helava, H. Short period superlattices of AlN/Al_{0.08}Ga_{0.92}N grown on AlN substrates. *Appl. Phys. Lett.* **2004**, *85*, 4355–4357. [[CrossRef](#)]
54. Borisov, B.; Nikishin, S.; Kuryatkov, V.; Temkin, H. Enhanced deep ultraviolet luminescence from AlGaIn quantum wells grown in the three dimensional mode. *Appl. Phys. Lett.* **2005**, *87*, 191902. [[CrossRef](#)]
55. Borisov, B.A.; Nikishin, S.A.; Kuryatkov, V.V.; Kuchinski, V.I.; Holtz, M.; Temkin, H. Enhanced radiative recombination in AlGaIn quantum wells grown by molecular-beam epitaxy. *Semiconductors* **2006**, *40*, 454–458. [[CrossRef](#)]
56. Panish, M.B.; Temkin, H. *Gas Source Molecular Beam Epitaxy. Growth and Properties of Phosphorus Containing III–V Heterostructures*; Springer Series in Materials Science; Springer: Berlin/Heidelberg, Germany, 1993; Volume 26, pp. 115–230. ISBN 3-540-56540-X (Berlin) or 0-387-56540-X (New York).
57. Nikishin, S.A.; Borisov, B.A.; Garrett, G.A.; Sarney, W.L.; Sampath, A.V.; Shen, H.; Wraback, M.; Holtz, M. Enhanced luminescence from Al_xGa_{1-x}N/Al_yGa_{1-y}N quantum wells grown by gas source molecular beam epitaxy with ammonia. *Proc. SPIE* **2007**, *6473*, 647306.
58. Nikishin, S.A.; Borisov, B.A.; Kuryatkov, V.V.; Holtz, M.; Garrett, G.A.; Sarney, W.L.; Sampath, A.V.; Shen, H.; Wraback, M. Correlations between the growth modes and luminescence properties of AlGaIn quantum structures. *Jpn. J. Appl. Phys.* **2008**, *47*, 1556–1558. [[CrossRef](#)]
59. Islam, S.M.; Lee, K.; Verma, J.; Protasenko, V.; Rouvimov, S.; Bharadwaj, S.; Xing, H.G.; Jena, D. MBE-grown 232–270 nm deep-UV LEDs using monolayer thin binary GaN/AlN quantum heterostructures. *Appl. Phys. Lett.* **2017**, *110*, 041108. [[CrossRef](#)]
60. Islam, S.M.; Protasenko, V.; Lee, K.; Rouvimov, S.; Verma, J.; Xing, H.G.; Jena, D. Deep-UV emission at 219 nm from ultrathin MBE GaN/AlN quantum heterostructures. *Appl. Phys. Lett.* **2017**, *111*, 091104. [[CrossRef](#)]
61. Chandolu, A.; Nikishin, S.; Holtz, M.; Temkin, H. X-ray diffraction study of AlN/AlGaIn short-period superlattices. *J. Appl. Phys.* **2007**, *102*, 114909. [[CrossRef](#)]
62. Kandaswamy, P.K.; Guillot, F.; Bellet-Amalric, E.; Monroy, E.; Nevou, L.; Tchernycheva, M.; Michon, A.; Julien, F.H.; Baumann, E.; Giorgetta, F.R.; et al. GaN/AlN short-period superlattices for intersubband optoelectronics: A systematic study of their epitaxial growth, design, and performance. *J. Appl. Phys.* **2008**, *104*, 093501. [[CrossRef](#)]
63. Kladko, V.; Kuchuk, A.; Lytvyn, P.; Yefanov, O.; Safriuk, N.; Belyaev, A.; Mazur, Y.I.; DeCuir, E.A., Jr.; Ware, M.E.; Salamo, G.J. Substrate effects on the strain relaxation in GaN/AlN short-period superlattices. *Nanoscale Res. Lett.* **2012**, *7*, 289. [[CrossRef](#)] [[PubMed](#)]
64. Noh, Y.-K.; Seo, J.-H.; Choi, H.-S.; Kim, M.-D.; Oh, J.-E. Thickness dependence of temperature-induced emission mechanism in InGaIn/AlGaIn short-period superlattices. *J. Appl. Phys.* **2012**, *112*, 043102. [[CrossRef](#)]
65. Kutt, R.N.; Shcheglov, M.P.; Ratnikov, V.V.; Yagovkina, M.A.; Davydov, V.Y.; Smirnov, A.N.; Rozhavskaia, M.M.; Zavarin, E.E.; Lundin, V.V. X-ray diffraction study of short-period AlN/GaN superlattices. *Crystallogr. Rep.* **2013**, *58*, 953–958. [[CrossRef](#)]
66. Piquier, C.; Frandon, J.; Demangeot, F.; Smirnov, M.; Sarua, A.; Kuball, M.; Monroy, E.; Daudin, B. Behavior of phonons in short-period GaN-AlN superlattices. *Phys. Stat. Sol.* **2004**, *1*, 2706–2710. [[CrossRef](#)]

67. Davydov, V.Yu.; Roginskii, E.M.; Smirnov, A.N.; Kitaev, Y.E.; Yagovkina, M.A.; Kyutt, R.N.; Rozhavskaia, M.M.; Zavarin, E.E.; Lundin, W.V.; Smirnov, M.B. Lattice dynamics of short-period AlN/GaN short period superlattices: Theory and experiments. *Phys. Stat. Sol.* **2013**, *210*, 484–487. [CrossRef]
68. Pankin, D.V.; Smirnov, M.B.; Davydov, V.Y.; Smirnov, A.N.; Zavarin, E.E.; Lundin, W.V. Elastic Strains and Delocalized Optical Phonons in AlN/GaN Superlattices. *Semiconductors* **2016**, *50*, 1043–1048. [CrossRef]
69. Sarkar, K.; Datta, D.; Gosztola, D.J.; Shi, F.; Nicholls, A.; Stroschio, M.A.; Dutta, M. Raman analysis of phonon modes in a short period AlN/GaN superlattice. *Superlattices Microstruct.* **2018**, *115*, 116–122. [CrossRef]
70. Stolyarchuk, N.; Markurt, T.; Courville, A.; March, K.; Tottereau, O.; Vennéguès, P.; Albrecht, M. Impact of sapphire nitridation on formation of Al-polar inversion domains in N-polar AlN epitaxial layers. *J. Appl. Phys.* **2017**, *122*, 155303. [CrossRef]
71. Schuck, P.J.; Mason, M.D.; Grober, R.D.; Ambacher, O.; Lima, A.P.; Miskys, C.; Dimitrov, R.; Stutzmann, M. Spatially resolved photoluminescence of inversion domain boundaries in GaN-based lateral polarity heterostructures. *Appl. Phys. Lett.* **2001**, *79*, 952–954. [CrossRef]
72. Shubina, T.V.; Jmerik, V.N.; Tkachman, M.G.; Vekshin, V.A.; Ratnikov, V.V.; Toropov, A.A.; Sitnikova, A.A.; Ivanov, S.V.; Bergman, J.P.; Karlsson, F.; et al. Nanometric-scale fluctuations of intrinsic electric fields in GaN/AlGaIn quantum wells with inversion domains. *Phys. Stat. Sol.* **2002**, *234*, 919–923. [CrossRef]
73. SiLENSe—Software Tool for Light Emitting Diode (LED) Bandgap Engineering. Available online: <https://na01.safelinks.protection.outlook.com/?url=http%3A%2F%2Fwww.str-soft.com%2Fproducts%2FSiLENSe%2Findex.htm&data=02%7C01%7CSergey.A.Nikishin%40ttu.edu%7C1b70d2ef115047f2580008d622bf3be0%7C178a51bf8b2049ffb65556245d5c173c%7C0%7C0%7C636734602099986989&sdata=YpequeQnoljnZ5cNkIA7U5Zts7E%2FGL0Jz%2F1oAfZEdX4%3D&reserved=0> (accessed on 22 November 2018).
74. Crosslight Software Inc. Available online: <https://na01.safelinks.protection.outlook.com/?url=https%3A%2F%2Fcrosslight.com%2F&data=02%7C01%7CSergey.A.Nikishin%40ttu.edu%7C1b70d2ef115047f2580008d622bf3be0%7C178a51bf8b2049ffb65556245d5c173c%7C0%7C0%7C636734602099986989&sdata=vCC9BOBAXHLNXsh6KhW1CvooXSMJOC2KdKHv77BAJl%3D&reserved=0> (accessed on 22 November 2018).
75. Synopsys, Inc. Available online: <https://na01.safelinks.protection.outlook.com/?url=https%3A%2F%2Fwww.synopsys.com%2F&data=02%7C01%7CSergey.A.Nikishin%40ttu.edu%7C1b70d2ef115047f2580008d622bf3be0%7C178a51bf8b2049ffb65556245d5c173c%7C0%7C0%7C636734602099986989&sdata=33YOp0jIN06RqaUg2AijE6oOB2OH%2Bi%2BNnzafC3Y2lgM%3D&reserved=0> (accessed on 22 November 2018).
76. Bandgap Engineering Superlattice Simulation Tool (BESST)—Package for Simulation of Optoelectronic Devices Based on Group-III Nitride superlattices. Available online: <http://www.str-soft.com/products/BESST/index.htm> (accessed on 22 November 2018).
77. Kozodoy, P.; Hansen, M.; DenBaars, S.P.; Mishra, U.K. Enhanced Mg doping efficiency in Al_{0.2}Ga_{0.8}N/GaN superlattices. *Appl. Phys. Lett.* **1999**, *74*, 3681–3683. [CrossRef]
78. Bulashevich, K.A.; Karpov, S.Y. Heterojunctions between group-III nitride short period superlattices. *Phys. Stat. Sol.* **2005**, *2*, 2394–2398. [CrossRef]
79. Holtz, M.; Prokofyeva, T.; Seon, M.; Copeland, K.; Vanbuskirk, J.; Williams, S.; Nikishin, S.; Tretyakov, V.; Temkin, H. Composition dependence of the optical phonon energies in hexagonal Al_xGa_{1-x}N. *J. Appl. Phys.* **2001**, *89*, 7977–7982. [CrossRef]
80. Kuryatkov, V.; Chandolu, A.; Borisov, B.; Kipshidze, G.; Zhu, K.; Nikishin, S.; Temkin, H.; Holtz, M. Solar-blind ultraviolet photodetectors based on superlattices of AlN/AlGa(In)N. *Appl. Phys. Lett.* **2003**, *82*, 1323–1325. [CrossRef]
81. Herzog, J.B.; Mintairov, A.M.; Sun, K.; Cao, Y.; Jena, D.; Merz, J.L. Infrared reflectivity spectroscopy of optical phonons in short-period AlGaIn/GaN superlattices. *Proc. SPIE* **2007**, *6648*, 664803.
82. Marx, G.; Engelbrecht, J.A.A.; Lee, M.E.; Wagener, M.C.; Henry, A. Comments on a peak of Al_xGa_{1-x}N observed by infrared reflectance. *Infrared Phys. Technol.* **2016**, *76*, 493–499. [CrossRef]
83. Pendlebury, S.T.; Lynam, P.; Mowbray, D.J.; Parbrook, P.J.; Wood, D.A.; Lada, M.; O'Neill, J.P.; Cullis, A.G.; Skolnick, M.S. Optical characterization of AlGaIn epitaxial layers and GaN/AlGaIn quantum wells. *Phys. Stat. Sol.* **2001**, *188*, 871–875. [CrossRef]

84. Adelman, C.; Sarigiannidou, E.; Jalabert, D.; Hori, Y.; Rouvière, J.-L.; Daudin, B.; Fanget, S.; Bru-Chevallier, C.; Shibata, T.; Tanaka, M. Growth and optical properties of GaN/AlN quantum wells. *Appl. Phys. Lett.* **2003**, *82*, 4154–4156. [[CrossRef](#)]
85. Paskov, P.; Monemar, B.; Kamyama, S.; Amano, H.; Akasaki, I. Optical Properties of undoped, n-doped and p-doped GaN/AlN superlattices. *Mater. Res. Soc. Symp. Proc.* **2007**, *955*, 0955-I12-03. [[CrossRef](#)]
86. Da-Bing, L.; Wei-Guo, H.; Hideto, M.; Kazumasa, H.; Hang, S. Enhanced deep ultraviolet emission from Si-doped $\text{Al}_x\text{Ga}_{1-x}\text{N}$ /AlN MQWs. *Chin. Phys. B* **2010**, *19*, 127891. [[CrossRef](#)]
87. Borisov, B.; Kuryatkov, V.; Kudryavtsev, Y.; Asomoza, R.; Nikishin, S.; Holtz, M.; Temkin, H. Si-doped $\text{Al}_x\text{Ga}_{1-x}\text{N}$ ($0.56 \leq x \leq 1$) layers grown by molecular beam epitaxy with ammonia. *Appl. Phys. Lett.* **2005**, *87*, 132106–132108. [[CrossRef](#)]
88. Taniyasu, Y.; Kasu, M.; Toshiaki Makimoto, T. Electrical conduction properties of n-type Si-doped AlN with high electron mobility ($>100 \text{ cm}^2 \text{ V}^{-1} \text{ s}^{-1}$). *Appl. Phys. Lett.* **2004**, *85*, 4672–4674. [[CrossRef](#)]
89. Contreras, S.; Konczewicz, L.; Messaoud, J.B.; Peyre, H.; Khalfioui, M.A.; Matta, S.; Leroux, M.; Damilano, B.; Brault, J. High temperature electrical transport study of Si-doped AlN. *Superlattices Microstruct.* **2016**, *98*, 253–258. [[CrossRef](#)]
90. Pampili, P.; Parbrook, P.J. Doping on III-nitride materials. *Mat. Sci. Semicond. Proc.* **2017**, *62*, 180–191. [[CrossRef](#)]
91. Nikishin, S.A.; Kuryatkov, V.V.; Chandolu, A.; Borisov, B.A.; Kipshidze, G.D.; Ahmad, I.; Holtz, M.; Temkin, H. Deep ultraviolet light emitting diodes based on short period superlattices of AlN/AlGa(In)N. *Jpn. J. Appl. Phys.* **2003**, *42*, L1362–L1365. [[CrossRef](#)]
92. Yun, J.; Choi, K.; Mathur, K.; Kuryatkov, V.; Borisov, B.; Kipshidze, G.; Nikishin, S.; Temkin, H. Low resistance ohmic contacts to digital alloys of n-AlGaIn/AlN. *IEEE Electron Device Lett.* **2006**, *27*, 22–24. [[CrossRef](#)]
93. Kozodoy, P.; Xing, H.; DenBaars, S.P.; Mishra, U.K.; Saxler, A.; Perrin, R.; Elhamri, S.; Mitchel, W.C. Heavy doping effects in Mg-doped GaN. *J. Appl. Phys.* **2000**, *87*, 1832–1835. [[CrossRef](#)]
94. Jiang, X.-H.; Shi, J.-J.; Zhang, M.; Zhong, H.-X.; Huang, P.; Ding, Y.-M.; He, Y.-P.; Cao, X. Reduction of the Mg acceptor activation energy in GaN, AlN, $\text{Al}_{0.83}\text{Ga}_{0.17}\text{N}$ and Mg_{Ga} δ -doping $(\text{AlN})_5/(\text{GaN})_1$: The strain effect. *J. Phys. D Appl. Phys.* **2015**, *48*, 475104. [[CrossRef](#)]
95. Nam, K.B.; Nakarmi, M.L.; Li, J.; Lin, J.Y.; Jiang, H.X. Mg acceptor level in AlN probed by deep ultraviolet photoluminescence. *Appl. Phys. Lett.* **2003**, *83*, 878–880. [[CrossRef](#)]
96. Liang, Y.-H.; Towe, E. Progress in efficient doping of high aluminum-containing group III-nitrides. *Appl. Phys. Rev.* **2018**, *5*, 011107. [[CrossRef](#)]
97. Ilegems, M.; Dingle, R. Luminescence of Mg- and Be- doped GaN. *J. Appl. Phys.* **1973**, *44*, 4234–4235. [[CrossRef](#)]
98. Gelhausen, O.; Phillips, M.R.; Goldys, E.M.; Paskova, T.; Monemar, B.; Strassburg, M.; Hoffmann, A. Dissociation of H-related defect complexes in Mg-doped GaN. *Phys. Rev. B* **2004**, *69*, 125210. [[CrossRef](#)]
99. Amano, H.; Kito, M.; Hiramatsu, K.; Akasaki, I. P-type conduction in Mg-doped GaN treated with low-energy electron beam irradiation (LEEBI). *Jpn. J. Appl. Phys.* **1989**, *28*, L2112–L2114. [[CrossRef](#)]
100. Chernyak, L.; Osinsky, A.; Fuflyigin, V.; Schubert, E.F. Electron beam-induced increase of electron diffusion length in n-type GaN and AlGaIn/GaN superlattices. *Appl. Phys. Lett.* **2000**, *77*, 875–877. [[CrossRef](#)]
101. Phillips, M.R.; Merklein, M.; Hardy, T.; Manning, T.J.; Wintrebert-Fouquet, M. A mechanism for Mg acceptor activation in GaN by low energy electron beam irradiation. *Microsc. Microanal.* **2010**, *16*, 816–817. [[CrossRef](#)]
102. Korotkov, R.Y.; Gregie, J.M.; Wessels, B.W. Electrical properties of p-type GaN:Mg codoped with oxygen. *Appl. Phys. Lett.* **2001**, *78*, 222–224. [[CrossRef](#)]
103. Kipshidze, G.; Kuryatkov, V.; Borisov, B.; Kudryavtsev, Y.; Asomoza, R.; Nikishin, S.; Temkin, H. Mg and O codoping in p-type GaN and $\text{Al}_x\text{Ga}_{1-x}\text{N}$ ($0 < x < 0.08$). *Appl. Phys. Lett.* **2002**, *80*, 2910–2912. [[CrossRef](#)]
104. Wu, R.Q.; Shen, L.; Yang, M.; Sha, Z.D.; Cai, Y.Q.; Feng, Y.P.; Huang, Z.G.; Wu, Q.Y. Enhancing hole concentration in AlN by Mg:O codoping: Ab initio study. *Phys. Rev. B* **2008**, *77*, 073203. [[CrossRef](#)]
105. Khan, M.A.; Adviarahan, V.; Zhang, J.P.; Chen, C.; Kuokstis, E.; Chitnis, A.; Shatalov, M.; Yang, J.W.; Simin, G. Stripe geometry ultraviolet light emitting diodes at 305 nanometers using quaternary AlInGaIn multiple quantum wells. *Jpn. J. Appl. Phys.* **2001**, *40*, L1308–L1310. [[CrossRef](#)]
106. Lopatiuk-Tirpak, O.; Chernyak, L.; Borisov, B.A.; Kuryatkov, V.V.; Nikishin, S.A.; Gartsman, K. Electron irradiation-induced increase of minority carrier diffusion length, mobility, and lifetime in Mg-doped AlN/AlGaIn short period superlattice. *Appl. Phys. Lett.* **2007**, *91*, 182103. [[CrossRef](#)]

107. Allerman, A.A.; Crawford, M.H.; Miller, M.A.; Lee, S.R. Growth and characterization of Mg-doped AlGa_xN-AlN short-period superlattices for deep-UV optoelectronic devices. *J. Cryst. Growth* **2010**, *312*, 756–761. [[CrossRef](#)]
108. Nikishin, S.; Borisov, B.; Mansurov, V.; Pandikunta, M.; Chary, I.; Rajanna, G.; Bernussi, A.; Kudryavtsev, Y.; Asomoza, R.; Bulashevich, K.A.; et al. Short period p-type AlN/AlGa_xN superlattices for deep UV light emitters. *Mater. Res. Soc. Symp. Proc.* **2010**, *1202*, 1202-I10-03. [[CrossRef](#)]
109. Shatalov, M.; Gaska, R.; Yang, J.; Shur, M. Method of Doping and Semiconductor Devices. U.S. Patent 8,426,225, 23 April 2013.
110. Martens, M.; Kuhn, C.; Ziffer, E.; Simoneit, T.; Kueller, V.; Knauer, A.; Rass, J.; Wernicke, T.; Einfeldt, S.; Weyers, M.; et al. Low absorption loss p-AlGa_xN superlattice cladding layer for current-injection deep ultraviolet laser diodes. *Appl. Phys. Lett.* **2016**, *108*, 151108. [[CrossRef](#)]
111. Suzuki, M.; Nishio, J.; Onomura, M.; Hongo, C. Doping characteristics and electrical properties of Mg-doped AlGa_xN grown by atmospheric-pressure MOCVD. *J. Cryst. Growth* **1998**, *189/190*, 511–515. [[CrossRef](#)]
112. Li, J.; Oder, T.N.; Nakarmi, M.L.; Lin, J.Y.; Jiang, H.X. Optical and electrical properties of Mg-doped p-type Al_xGa_{1-x}N. *Appl. Phys. Lett.* **2002**, *80*, 1210–1212. [[CrossRef](#)]
113. Taniyasu, Y.; Kasu, M.; Makimoto, T. An aluminium nitride light-emitting diode with a wavelength of 210 nanometres. *Nature* **2006**, *441*, 325–328. [[CrossRef](#)] [[PubMed](#)]
114. Kinoshita, T.; Obata, T.; Yanagi, H.; Inoue, S.-I. High p-type conduction in high-Al content Mg-doped AlGa_xN. *Appl. Phys. Lett.* **2013**, *102*, 012105. [[CrossRef](#)]
115. Dussaigne, A.; Damilano, B.; Brault, J.; Massies, J.; Feltn, E.; Grandjean, N. High doping level in Mg-doped GaN layers grown at low temperature. *J. Appl. Phys.* **2008**, *103*, 013110. [[CrossRef](#)]
116. Chuang, S.L.; Chang, C.S. k-p method for strained wurtzite semiconductors. *Phys. Rev. B* **1996**, *54*, 2491–2504. [[CrossRef](#)]
117. Blank, T.V.; Gol'dberg, Y.A. Mechanisms of current flow in metal-semiconductor ohmic contacts. *Semiconductors* **2007**, *41*, 1263–1292. [[CrossRef](#)]
118. Ho, J.-K.; Jong, C.-S.; Chiu, C.C.; Huang, C.-N.; Shih, K.-K.; Chen, L.-C.; Chen, F.-R.; Kai, J.-J. Low-resistance ohmic contacts to p-type GaN achieved by the oxidation of Ni/Au films. *J. Appl. Phys.* **1999**, *86*, 4491. [[CrossRef](#)]
119. Lim, S.-H.; Ra, T.-Y.; Kim, W.-Y. Interface observation in Au/Ni/p-GaN studies by HREM and energy-filtering TEM. *J. Electron Microsc.* **2003**, *52*, 459–464. [[CrossRef](#)]
120. Qiao, D.; Yu, L.S.; Lau, S.S.; Lin, J.Y.; Jiang, H.X.; Haynes, T.E. A study of the Au/Ni ohmic contact on p-GaN. *J. Appl. Phys.* **2000**, *88*, 4196–4200. [[CrossRef](#)]
121. Chary, I.; Chandolu, A.; Borisov, B.; Kuryatkov, V.; Nikishin, S.; Holtz, M. Influence of surface treatment and annealing temperature on the formation of low-resistance Au/Ni ohmic contacts to p-GaN. *J. Electron. Mater.* **2009**, *38*, 545–550. [[CrossRef](#)]
122. Chary, I.; Borisov, B.; Kuryatkov, V.; Kudryavtsev, Y.; Asomoza, R.; Nikishin, S.; Holtz, M. Low resistance ohmic contacts to p-type GaN and AlGa_xN. *Mater. Res. Soc. Symp. Proc.* **2009**, *1108*, 1108-A09-30.
123. Nikishin, S.; Chary, I.; Borisov, B.; Kuryatkov, V.; Kudryavtsev, Y.; Asomoza, R.; Karpov, S.Y.; Holtz, M. Mechanism of carriers injection in (Ni/Au)/p-Al_xGa_{1-x}N:Mg (0 ≤ x < 0.1) ohmic contacts. *Appl. Phys. Lett.* **2009**, *95*, 163502. [[CrossRef](#)]
124. Nikishin, S.; Borisov, B.; Kuryatkov, V.; Usikov, A.; Dmitriev, V.; Holtz, M. Deep UV AlGa_xN light emitting diodes grown by gas source molecular beam epitaxy on sapphire and AlGa_xN/sapphire substrates. *Proc. SPIE* **2006**, *6121*, 6121OT-1-16. [[CrossRef](#)]
125. Moustakas, T.D.; Liao, Y.; Kao, C.-K.; Thomidis, C.; Bhattacharyya, A.; Bhattarai, D.; Noldawer, A. Deep UV LEDs with high IQE based on AlGa_xN alloys with strong band structure potential fluctuations. *Proc. SPIE* **2012**, *8278*, 8278OL-1-11. [[CrossRef](#)]
126. Rass, J.; Kolbe, T.; Ploch, N.L.; Wernicke, T.; Mehnke, F.; Kuhn, C.; Enslin, J.; Guttman, M.; Reich, C.; Mogilatenko, A.; et al. High power UV-B LEDs with long lifetime. *Proc. SPIE* **2015**, *9363*, 93631K-1-13. [[CrossRef](#)]
127. Mondal, R.K.; Chatterjee, V.; Singh, S.; Islam, S.M.; Pal, S. Optimization of structural parameters for highly efficient AlGa_xN based deep ultraviolet light emitting diodes. *Superlattices Microstruct.* **2017**, *112*, 339–352. [[CrossRef](#)]

128. Liu, M.; Zhou, S.; Liu, X.; Gao, Y.; Ding, X. Comparative experimental and simulation studies of high-power AlGaIn-based 353 nm ultraviolet flip-chip and top-emitting LEDs. *Jpn. J. Appl. Phys.* **2018**, *57*, 031001. [[CrossRef](#)]
129. Bulashevich, K.A.; Ramm, M.S.; Karpov, S.Yu. Effects of electron and optical confinement on performance of UV laser diodes. *Phys. Stat. Sol.* **2009**, *6*, 603–606. [[CrossRef](#)]
130. Liang, Y.-H.; Towe, E. Heavy Mg-doping of (AlGa)N films for potential applications in deep ultraviolet light-emitting structures. *J. Appl. Phys.* **2018**, *123*, 095303. [[CrossRef](#)]
131. Park, J.H.; Kim, J.K.; Cho, J. Observation of space-charge-limited current in AlGaIn/GaN ultraviolet light emitting diodes. *Mater. Lett.* **2018**, *214*, 217–219. [[CrossRef](#)]
132. Liu, D.; Cho, S.J.; Park, J.; Seo, J.-H.; Dalmau, R.; Zhao, D.; Kim, K.; Gong, J.; Kim, M.; Lee, I.-K.; et al. 229 nm UV LEDs on aluminum nitride single crystal substrates using p-type silicon for increased hole injection. *Appl. Phys. Lett.* **2018**, *112*, 081101. [[CrossRef](#)]



© 2018 by the author. Licensee MDPI, Basel, Switzerland. This article is an open access article distributed under the terms and conditions of the Creative Commons Attribution (CC BY) license (<http://creativecommons.org/licenses/by/4.0/>).